High-resolution Rayleigh-wave velocity maps of central Europe from a dense ambient-noise data set

J. Verbeke, Lapo Boschi, L. Stehly, E. Kissling, A. Michelini

Geophysical Journal International

Geophys. J. Int. (2012) **188,** 1173–1187 doi: 10.1111/j.1365-246X.2011.05308.x

High-resolution Rayleigh-wave velocity maps of central Europe from a dense ambient-noise data set

J. Verbeke,[1] L. Boschi,[1,2] L. Stehly,[3] E. Kissling[1] and A. Michelini[4]

[1] *Institute of Geophysics, ETH, Sonneggstr.* 5, 8092 *Zürich, Switzerland. E-mail: verbeke@tomo.ig.erdw.ethz.ch*
[2] *Institute of Theoretical Physics, University of Zürich, Winterthurerstr.* 190, 8057 *Zürich, Switzerland*
[3] *Géoazur, Bât.* 4, 250 *rue Albert Einstein, Les Lucioles* 1, *Sophia Antipolis,* 06560 *Valbonne, France*
[4] *INGV, via di Vigna Murata* 605, 00143 *Rome, Italy*

Accepted 2011 November 17. Received 2011 October 25; in original form 2011 June 7

SUMMARY

We present a new database of surface wave group and phase-velocity dispersion curves derived from seismic ambient noise, cross-correlating continuous seismic recordings from the Swiss Network, the German Regional Seismological Network (GRSN), the Italian national broad-band network operated by the Istituto Nazionale di Geosica e Vulcanologia (INGV). To increase the aperture of the station array, additional measurements from the Mediterranean Very Broad-band Seismographic Network (MedNet), the Austrian Central Institute for Meteorology and Geodynamics (ZAMG), the French, Bulgarian, Hungarian, Romanian and Greek stations obtained through Orfeus are also included. The ambient noise, we are using to assemble our database, was recorded at the above-mentioned stations between 2006 January and 2006 December. Correlating continuous signal recorded at pairs of stations, allows to extract coherent surface wave signal travelling between the two stations. Usually the ambient-noise cross-correlation technique allows to have informations at periods of 30 s or shorter. By expanding the database of noise correlations, we seek to increase the resolution of the central Europe crustal model.

We invert the resulting data sets of group and phase velocities associated with 8–35 s Rayleigh waves, to determine 2-D group and phase-velocity maps of the European region. Inversions are conducted by means of a 2-D linearized tomographic inversion algorithm. The generally good agreement of our models with previous studies and good correlation of well-resolved velocity anomalies with geological features, such as sedimentary basins, crustal roots and mountain ranges, documents the effectiveness of our approach.

Key words: Surface waves and free oscillations; Seismic tomography; Crustal structure; Europe.

1 INTRODUCTION

The European lithosphere is shaped by the convergence of the African and European plates involving between them a mosaic of microplates of oceanic and continental lithosphere (Schmid *et al.* 2004; Boschi *et al.* 2010). The resulting strong 3-D heterogeneities in crust and upper mantle are naturally difficult to image seismically. Yet, reliable seismic 3-D lithosphere models are necessary for accurate earthquake locations, and as constraints for geodynamic modelling. Most published tomographic models are based on observations of *P*-wave traveltimes (e.g. Bijwaard & Spakman 2000; Lippitsch *et al.* 2003) or surface wave dispersion recorded from teleseimic events (e.g. Boschi *et al.* 2009, 2010; Chang *et al.* 2010). Teleseismic body waves are appropriate for imaging mantle structure, but they are only partially sensitive to the crustal-lithospheric depth range (Schivardi & Morelli 2009). High-frequency signals associated with teleseismic surface waves are generally weak, and high-quality measurements are only available at periods equal to or higher than 30 s. An alternative method is local earthquake tomography (LET), well-suited to image strong lithosphere heterogeneities in 3-D (e.g. Diehl *et al.* 2009; Di Stefano *et al.* 2009) but the relative scarcity of seismic events in large regions of Europe prevents LET to be consistently applied on a regional scale. Moreover, high quality local earthquake *S* data are difficult to pick (Diehl *et al.* 2009) and have not been used yet. Accurate maps of Moho depth and local crustal structure can be obtained by controlled source seismology (CSS) (Waldhauser *et al.* 1998, 2002), but although good at identifying crustal geometries, like the Moho discontinuity, CSS yields relatively few informations on lateral variation of *S*-velocity structure; moreover, CSS is a 2-D method and needs 3-D migration because sources and receivers are on the same side of the target structure. In summary,

'traditional' imaging techniques, applied individually have been insufficient to provide a high-resolution image of crustal and lithospheric *P*- and *S*-wave velocity structure at the scale of Europe.

A promising complementary seismic approach to enhance resolution of the shallow earth-wave velocity field is the so-called 'ambient-noise' technique. The ambient-noise method is based on the theoretical result that the cross-correlation of ambient seismic signal observed at two locations is generally very close, if not exactly coincident, with the Green's function associated with those locations (one being treated as the source, the other as the receiver; Weaver & Lobkis 2001; Snieder 2004).

The technique was first used in helioseismology (Duvall *et al.* 1993) to interpret oscillations observed at the surface of the Sun in terms of propagating waves. Weaver & Lobkis (2001) base their acoustic-wave treatment on the assumption of equipartition between all the modes of the propagation medium, which yields the equality between the derivative of the displacement Green's function and ambient-noise cross-correlation. Sanchez-Sesma & Campillo (2006) extended this result to the case of seismic waves. Snieder (2004) came to similar conclusions following the stationary-phase approach: if the station pair is surrounded by seismic sources at all azimuths (representative of a diffuse or equipartitioned seismic wavefield), the cross-correlation of cumulative recorded noise implicitly cancels out the contribution of sources that are not aligned with the station–station azimuth, and the surviving signal corresponds, again, to surface wave propagation along the station–station azimuth. Later, Wapenaar (2004) proved the connection between Green's function and ambient-noise correlation through an application of the reciprocity theorem. All theoretical studies are based on either of the following assumptions: (i) that (from a standing-wave viewpoint) noise be equipartitioned over all modes and (ii) that (from a travelling-wave viewpoint) the wavefield be diffuse, as a result of strong scattering and/or a geographically uniform distribution of noise sources.

Useful analyses of the performance of ambient-noise cross-correlation techniques in the real world, that is, in the absence of noise equipartition, are provided, for example, by Weaver *et al.* (2009), Cupillard & Capdeville (2010), Froment *et al.* (2010) and Tsai (2010). It has been noted that ambient-noise measurements are sensitive not only to the azimuthal distribution of the sources, but also to their distance from the station array (Harmon *et al.* 2008; Cupillard & Capdeville 2010). The importance of scattering has been verified, at least at the local scale and relatively high frequency (Gouédard *et al.* 2008; Froment *et al.* 2010). Tromp *et al.* (2010) have proposed an 'adjoint', numerical approach to quantify the effects of non-uniformity in the noise-source distribution, and to compute sensitivity kernels that account for such effects; the database presented in our study is currently being used by (Basini *et al.* 2011) in one of the first practical applications of this method.

In general, the high correlation between ambient-noise-based tomography and independent results in various, densely instrumented regions of the world suggests that real-world conditions are often sufficient: successful examples are California (Shapiro *et al.* 2005) and Europe (Yang *et al.* 2007; Stehly *et al.* 2009), where group velocities were measured, or Tibet (Yao *et al.* 2008), where phase velocities were measured.

The distribution of ambient-noise sources averaged on several months is sufficiently homogeneous to apply this method to image at crustal scale. We now know that observed surface wave ambient noise is only generated at the Earth's surface, and essentially over the oceans (storms, and the coupling of oceans with the solid Earth; Stehly *et al.* 2006), with most released energy roughly between 5 and 20 s. In the case of Europe, ambient noise comes mostly from the Atlantic, and only marginally from the Mediterranean Sea (Stehly *et al.* 2006; Chevrot *et al.* 2007; Kedar *et al.* 2008; Yang & Ritzwoller 2008).

With this study, we build on the earlier works of Stehly *et al.* (2009) and Li *et al.* (2010), compiling a larger database of surface wave dispersion measured by noise cross-correlation of European stations. The size of our region of interest is double that of either of those previous studies as it includes Germany, Switzerland and the Alpine region, Italy and the Tyrrhenian Sea. The earlier study of Yang *et al.* (2007) is similar to ours in that it covers a wider region but includes fewer stations; it is limited to lower frequencies and group-, rather than phase-velocity observations.

Since 2006, Italy is covered by a very dense network of at least 125 broad-band instruments. Combined with the central Europe stations already used by Stehly *et al.* (2009), a cumulative array of 196 receivers provides a coverage of crust and lithosphere unprecedented in Europe (Fig. 1). With this station array the Alps and the Po plain, where the regions of interest of Li *et al.* (2010) and Stehly *et al.* (2009) overlap, can be imaged with significantly better resolution than in either earlier study. Importantly, the large number of available high-quality observations allows us to observe not only group-, but also phase-velocity dispersion, and to extend our observations to relatively long periods of up to 35 s. The ultimate goal of this latter effort is to fill the gap between teleseismic and ambient-noise techniques of surface wave observation. Improving the reliability of ambient-noise-based dispersion curve at periods equal or higher than 30 s, somewhat too short for teleseismic observations, is equivalent to significantly improving seismic coverage of the lithosphere–asthenosphere boundary.

In the following, we first discuss the set of stations and associated seismic records that we used. We next describe the processing algorithm (similar to Bensen *et al.* 2007; Stehly *et al.* 2009) that we followed to extract, from such seismic records, estimates of the station–station Green's functions, and, subsequently, of the station–station group and phase velocities. We proceed with several synthetic tests to assess quantitatively the resolution of our data set. We apply phase-velocity tomography (e.g. Boschi 2006) to measure group- and phase-velocity dispersion data at periods between 8 and 35 s, to derive from our data, a set of 2-D maps of crustal and lithospheric structure of the region of interest. Our results are generally consistent with those of Li *et al.* (2010) and Stehly *et al.* (2009), which were both limited to smaller areas and/or to lower resolution. Our short period group- and phase-velocity maps are characterized by few small-scale features, which appear to be in good agreement with the geology of the region; our longer period group and phase-velocity maps correlate very well with a Moho map recently established from CSS and LET results from Wagner *et al.* (2011).

2 FROM CONTINUOUS RECORDS TO DISPERSION CURVES

As described by Stehly *et al.* (2006), one year of continuous recording is needed for the successful application of the ambient-noise method to regional-scale seismology. Over one year, seasonal effects associated with the geography of ocean storms cancel out, and the cumulative source distribution of stacked data is closer to being uniform: a condition for our cross-correlations to approximate the Green's functions well. To improve on our current knowledge of the European lithosphere, we combine and cross-correlate recordings

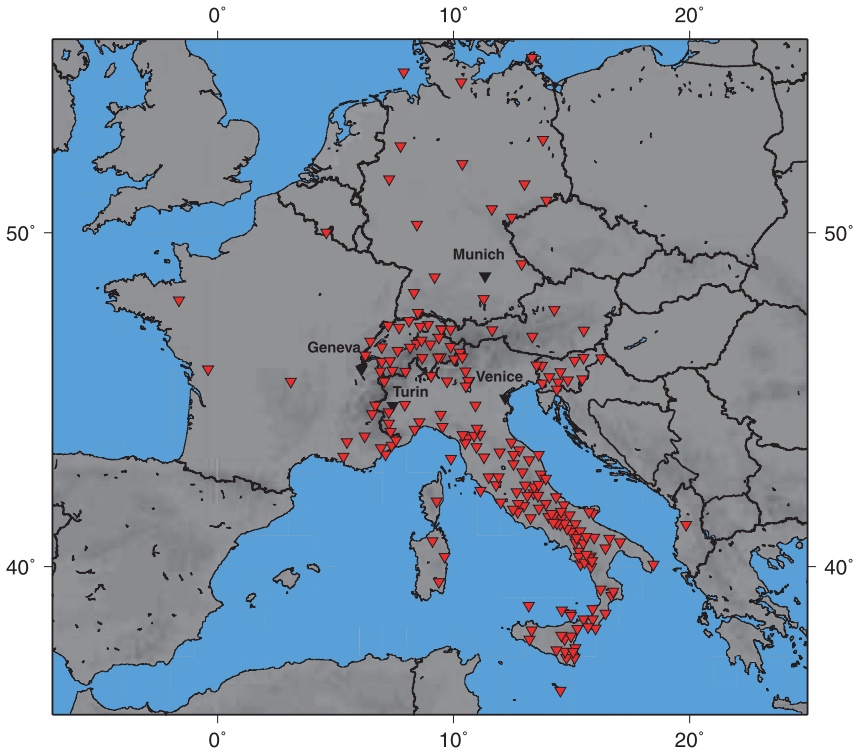

Figure 1. Location of the broad-band stations used in this study, from the combination of regional European networks detailed in Section 2.

from several broad-band European networks. We developed a new database of surface wave group- and phase-velocity dispersion curves, which we obtained by cross-correlating continuous seismic recordings mostly from the Swiss Network, the German Regional Seismological Network (GRSN), the Italian national broad-band network operated by the Istituto Nazionale di Geosica e Vulcanologia (INGV). To increase the aperture of the station array, we included additional measurements from the Mediterranean Very Broad-band Seismographic Network (MedNet), the Austrian Central Institute for Meteorology and Geodynamics (ZAMG), the French Broad-band Seismological Network and the Slovenia Seismic Network. The resulting station distribution is illustrated in the Fig. 1. We aimed at collecting continuous recordings for all these stations starting in 2006 January and until 2006 December, though of course not all stations were constantly operational in this time interval.

2.1 Sampling, whitening and emergence of coherent surface wave signal

We compute our correlations in the same way as Bensen *et al.* (2007) and Stehly *et al.* (2009). Bensen *et al.* (2007) extract Rayleigh-wave velocities from the cross-correlation of vertical with vertical, and radial with radial components recorded at the two stations; whereas Stehly *et al.* (2009) used the four possible combinations of cross-correlation between the vertical and radial component of the two stations (Z–Z, R–R, Z–R and R–Z) and then extract eight velocities measurements and averaged them to obtain the velocity between the two stations. In our study, we used only the vertical component of the record. The signal on the vertical component is more energetic than on the radial one; the radial component could additionally be affected by azimuthal anisotropy or by bending of Love-wave paths caused by lateral heterogeneity. Limiting our analysis to the vertical signal is a way to avoid all these potential issues.

The continuous data that are analysed here were recorded by broad-band stations, deployed with the primary goal of recording earthquakes and all the associated information. Because we are interested only in the diffuse, 'background' signal, our processing of the data is aimed at emphasizing what traditional seismology normally neglects as 'noise' (Bensen *et al.* 2007). We first remove trend, mean and instrumental response from the signal. We know through numerous previous studies that the spectrum of seismic ambient noise is not flat in the frequency domain (e.g. Bensen *et al.* 2007) but characterized by several peaks. All complexities in the spectrum of noise sources should be somehow corrected for, to better satisfy the requirement of equipartition (Section 1). We achieve this by systematically whitening the noise signal. Even though the resulting spectrum is not completely flat, the amplitude of the mentioned peaks and the bias towards longer periods are reduced.

Our cross-correlation algorithm consists of the following steps: (i) we divide the continuous records in large sets of day-long files; (ii) we cross-correlate the vertical component for all possible pairs of stations and for each day and (iii) we stack together the resulting daily station–station cross-correlations over the whole year. A separate stack is calculated for each available station pair. The result of this exercise, for stations AIGLE and ARBF, is shown in Fig. 2 as an example. As noise comes, at different times, from different predominant azimuths, stacking is equivalent to combining the effects of sources located at different azimuths: the stacked signal is, thus, closer to the required assumption of source uniformity/equipartition. At the same time, the effect of 'ballistic' waves coming from a single direction (e.g. an earthquake) will naturally

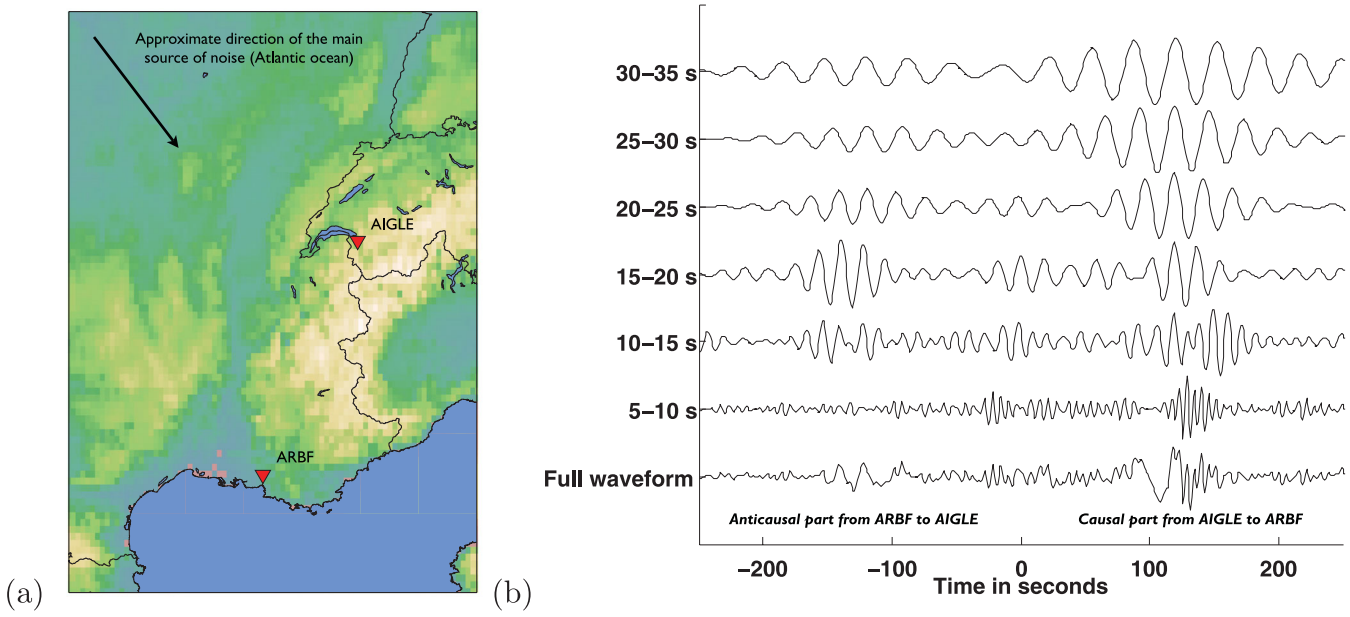

Figure 2. (a) Locations of stations AIGLE (western Switzerland) and ARBF (southern France). (b) Cross-correlation of stacked continuous signal (Section 2.1) recorded at AIGLE and ARBF, filtered over different frequency bands as indicated.

tend to cancel out: we don't need to artificially remove days of important seismic activity before processing the data. Our choice of sampling rate for the cross-correlation is determined by the type of structure that we are looking for. Because we are ultimately aiming at crustal/lithosphere-scale seismic imaging, our target is roughly the 0.025–0.5 Hz frequency range. On the basis of the Shannon's theorem, we need a sampling rate that is approximately twice the frequency of interest: we choose a sampling rate of 1 Hz. [In practice, our analysis is limited to somewhat lower frequencies (∼0.2 Hz) as a consequence of a fairly large average interstation distance of ∼100 km.]

As seen in Fig. 2, noise cross-correlations tend to be characterized by two symmetric maxima, one at positive and the other at negative time. These two portions of the cross-correlated signals are respectively dubbed causal and anticausal, as illustrated in fig. 1 of Stehly *et al.* (2006). Essentially, the causal part corresponds to energy propagating from AIGLE to ARBF and the anticausal one to energy propagating from ARBF to AIGLE. Note that, regardless of the frequency band at which the cross-correlation was filtered, a systematic difference in amplitude is evident between the causal and anticausal parts of the traces in Fig. 2, with causal parts showing larger amplitude than the anticausal ones. We infer that most ambient-noise energy propagates from the north to the south. This observation is consistent with what we found at other European station pairs, and confirms that most seismic ambient noise recorded in Europe is generated in the Atlantic ocean (e.g. Stehly *et al.* 2006, 2009).

We see in Fig. 2 a clear asymmetry in the amplitude of the causal and anticausal parts of the cross-correlations, at all period bands except 15–20 s. The surface waves on the causal and anticausal part have a similar traveltime for all period bands. We are interest of the phase and not of the amplitude. It is, thus, possible to obtain a good-quality measurement of dispersion, because dispersion is essentially related to phase and not amplitude. For the station pair of Fig. 2, as well as for most other station pairs in our study region, the asymmetry is minor compared to the overall cross-correlation signal, indicating that the source distribution is sufficiently close to uniform for the ambient noise to hold.

2.2 Analysis of dispersion

In the ambient-noise formalism assumed here, cross-correlations of stacked signal at a station pair are approximately coincident with the surface wave Green's function between the two stations (i.e. one station can be thought of as the source and the other as the receiver), and can be treated as such. It is, thus, legitimate to apply the frequency–time analysis (FTAN) method (Levshin *et al.* 1989; Ritzwoller & Levshin 1998; Bensen *et al.* 2007) to our cross-correlation, and measure the surface wave dispersion between all cross-correlated station pairs. Before applying the FTAN, we fold the causal and anticausal part on top of each other. We first apply a phase-matched filter to remove possible contamination of energy by higher modes and to increase the signal-to-noise ratio (SNR; Herrin & Goforth 1977; Bensen *et al.* 2007). Similar to Fig. 2, the FTAN then consists of bandpass filtering the signal around the different frequencies we want to measure (vertical axis in the bottom panel of Fig. 3) and plotting it as a function of time and frequency as shown in Fig. 3. The FTAN is used to measure group velocity. We identify, at each frequency, the maximum of the resulting envelope of signal amplitude and find the corresponding group velocity as the ratio of time to the known interstation distance: the group velocity as a function of frequency, that is, the dispersion curve, is found. We pick manually the amplitude maximum. In certain cases, it is not possible to identify it at all frequencies and we only make measurements in the frequency range where the maximum is sufficiently well defined: in practice, we measure SNR by comparing the peak of the cross-correlation waveform (corresponding to the peak of the Green's function) and divide by the pick of a time window of the same waveform well away from the Green's function. We then, only measure group velocity on cross-correlation with SNR of 5 or larger. We repeat our measurement procedure for all station pairs in our database, and show in Table 1 the number of group-velocity

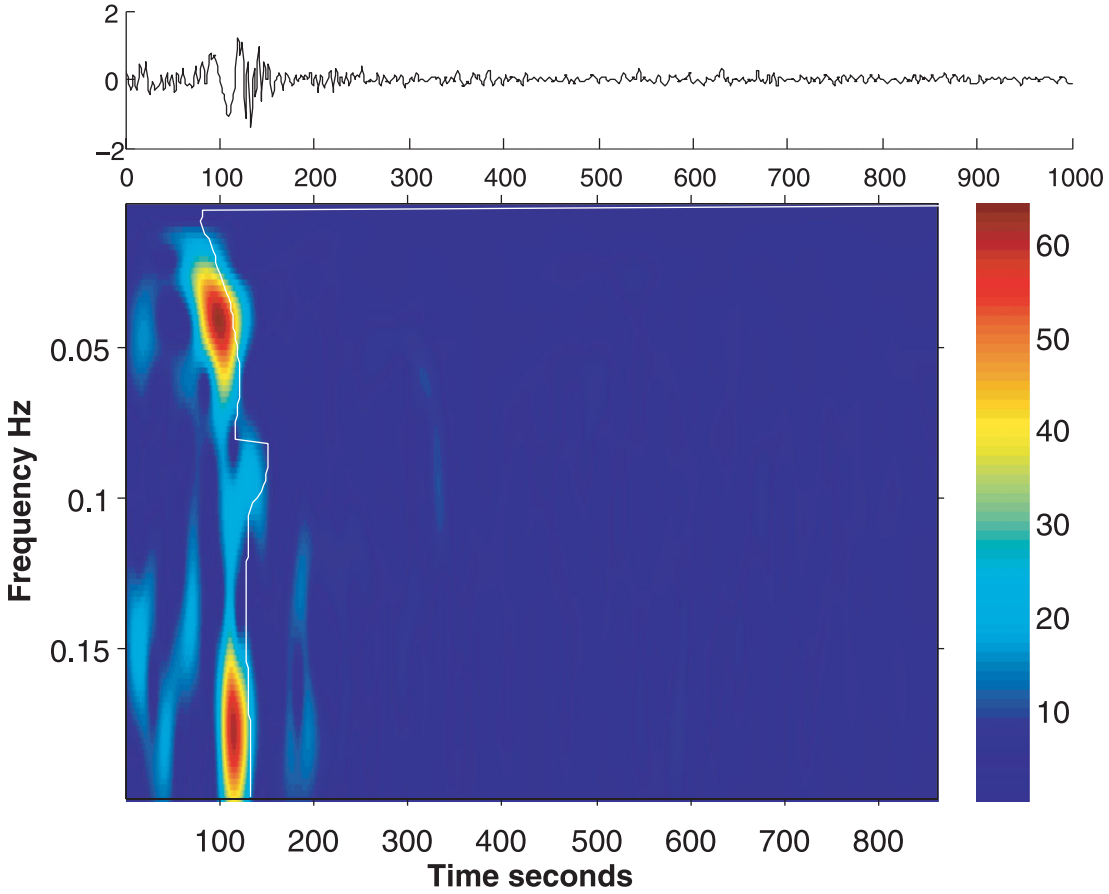

Figure 3. Frequency–time analysis applied to the cross-correlation of continuous records at AIGLE and ARBF (station locations are shown in Fig. 2).

Table 1. Number of station–station group-velocity observations included in our database. The total number of possible station–station combinations is 19 110.

Period	Number of data
8 s	4357
12 s	5822
16 s	6917
24 s	5512
30 s	3311
35 s	2890

observations that we finally keep for each analysed period. As a general rule, higher quality observations correspond to station couples with a longer available time window for cross-correlation (typically larger than 300 days for the large majority of the measurements included in our database).

Although the main focus of this paper is the development of a new group-velocity database, it is also useful to measure phase velocity to better constrain the *S* velocity of the crust, because the two types of measurements are well known to be sensitive at different depth (e.g. Ritzwoller *et al.* 2001). We measure phase velocity via the 2-station method as implemented by Meier *et al.* (2004). This method was originally designed to resolve local structure based on surface wave recordings of distant earthquakes. Instead of cross-correlation of earthquake signals, we apply it here to our cross-correlations of background noise. According to Meier *et al.* (2004), given the phase of the cross-correlation function, ϕ, as a function of frequency, ω, we obtain a phase-velocity dispersion curve via the formula

$$c(\omega) = \frac{\omega \Delta}{\arctan\{\Im[\phi(\omega)]/\Re[\phi(\omega)]\} + 2n\pi}, \quad (1)$$

where c denotes phase velocity, Δ the interstation distance and $\Re$ and $\Im$ the real and imaginary parts of the cross-correlation. The integer number, n, accounts for the ambiguity of the arctangent function, whose associated error on phase is a multiple of a full cycle 2π (Meier *et al.* 2004). In practice, as illustrated in Fig. 4, we need to implement eq. (1) for a set of possible values of $n = 0, 1, 2, \ldots$ and then, following Fry *et al.* (2010), we pick the dispersion curve closest to that predicted by PREM. Again, we only measure phase velocity on cross-correlations with a SNR of 5 or higher.

3 SURFACE WAVE TOMOGRAPHY

We derive group- and phase-velocity maps from the databases described earlier, applying the ray-theory formulation of Boschi & Dziewonski (1999). As long as effects caused by non-uniformity in the noise source distribution (e.g. Tromp *et al.* 2010) are neglected, our group- and phase-velocity databases can be treated as traditional ones, with our station pairs corresponding to the source-station pairs of earthquake-based tomography. The region of interest is subdivided into approximately equal-area pixels whose size would be $0.3^\circ \times 0.3^\circ$ at the equator; their longitudinal extent is corrected to keep the area approximately constant. Only pixels in the region of interest are sampled by the data and contribute to the inverse

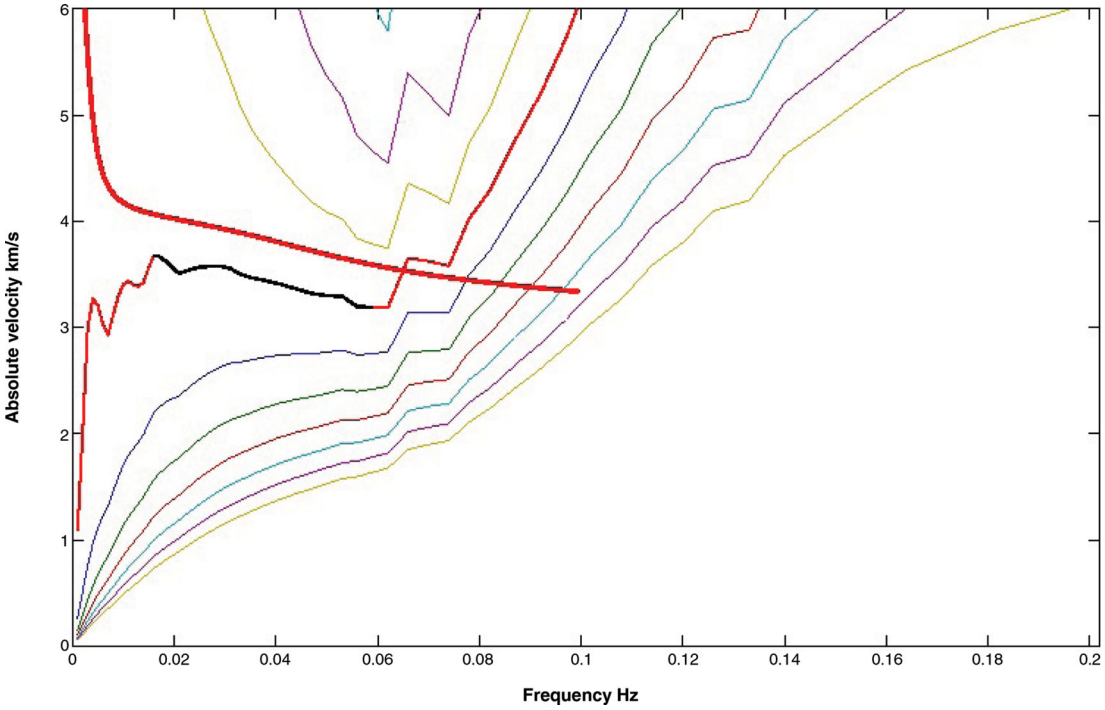

Figure 4. Phase-velocity dispersion curve from cross-correlation of the continuous recordings made at AIGLE and ARBF. Different coloured thin curves are the different dispersion curves corresponding to different values of n. The thick red curve is the theoretical dispersion curve derived from PREM model. The thin red curve correspond to $n = 0$ and turns out to be our preferred one. The black portion of this curve denotes the frequency range where we trust the measurement.

problem. A linear system is set up as described by Boschi & Dziewonski (1999) and solved in least-squares sense via the LSQR algorithm of Paige & Saunders (1982). The inverse problem is non-unique and regularized via roughness minimization.

The use of ray theory implicitly limits the resolution of our surface wave group- and phase-velocity maps to heterogeneities of wavelength comparable to, or larger than that of the inverted data. In 2-D surface wave tomography, the limits of ray-theory and the improvement to be expected from the application of finite-frequency methods are analysed in detail (though at longer wavelength). by Peter *et al.* (2009). We choose here to use a simple ray theory algorithm and derive approximate maps to evaluate the quality and information content of the data.

3.1 Resolution

We use ray theory to invert group- and phase-velocity measurements made at periods between 8 and 35 s. This poses the theoretical limit of resolution correspondingly between 20 and 130 km. In practice, resolution depends on the geographic coverage of our database. We quantify the resolution through a set of synthetic data inversions (e.g. Kissling 1988; Boschi & Dziewonski 1999). We first define a 'checkerboard' input group-velocity map coinciding with the spherical harmonic function of degree 60 and order 30, corresponding to anomalies extending a few hundred kilometres laterally and compute the corresponding synthetic phase anomalies by a simple matrix multiplication. No noise is added to the data. We invert the resulting synthetic data through an application of the same tomography algorithm that we use on real observations, including the regularization scheme and weight. The results of this exercise are illustrated in Fig. 5. At this stage, resolution limits associated with the approximations inherent to our theoretical formulation (ray theory, which is only strictly valid in the infinite-frequency limit) are neglected, and resolving power is independent of frequency. Because, for our data set, different surface wave frequencies have approximately the same geographic coverage, it is then unnecessary to repeat this exercise at all considered surface wave modes, and we only show in Fig. 5 results for 8 and 35 s group velocity. The input (Figs 5a and d) and output (Figs 5b and e) models are shown together with the density of ray paths at each period. Generally, the relatively long wavelength pattern of group-velocity heterogeneity is reproduced well throughout the region that is most densely covered by stations (Fig. 1), from northern Germany all the way down to the Tyrrhenian Sea. There is, however, a clear loss in recovered amplitude, which is a systematic problem in damped seismic tomography. The locations marked 1, 2 and 3 on the map are areas of high sensitivity of our data where anomalies are well recovered. Locations 5 and 6 are clearly affected by strong smearing artefacts due to very low ray coverage (Figs 5c and f). In area 4, the results from the two frequencies show different level of recoverage even if the region is covered by stations. Looking at the density of ray paths at that specific location, 35 s shows more ray paths (Fig. 5f) than 8 s, and indeed the anomaly in location 4 is better resolved.

To evaluate our algorithms power to resolve structures like we might observe in the real Earth, we perform a characteristic model test (Husen *et al.* 2009), replacing the checkerboard input model of Fig. 5(a) with a model containing randomly distributed (in 2-D) velocity anomalies of various sizes. Namely, we generate a 128×128-pixel image, with random values of velocity anomaly ranging between -1 and 1 per cent with respect to velocity as predicted by the Preliminary Reference Earth Model (PREM) (Dziewonski & Anderson 1981), apply a 2-D Fourier transform to the image, filter it in the Fourier domain so that heterogeneities of scalelength similar to those actually observed become dominant and inverse-Fourier-transform it back to the spatial domain. The resulting synthetic model is shown in Fig. 6 and contains anomalies of 100 km

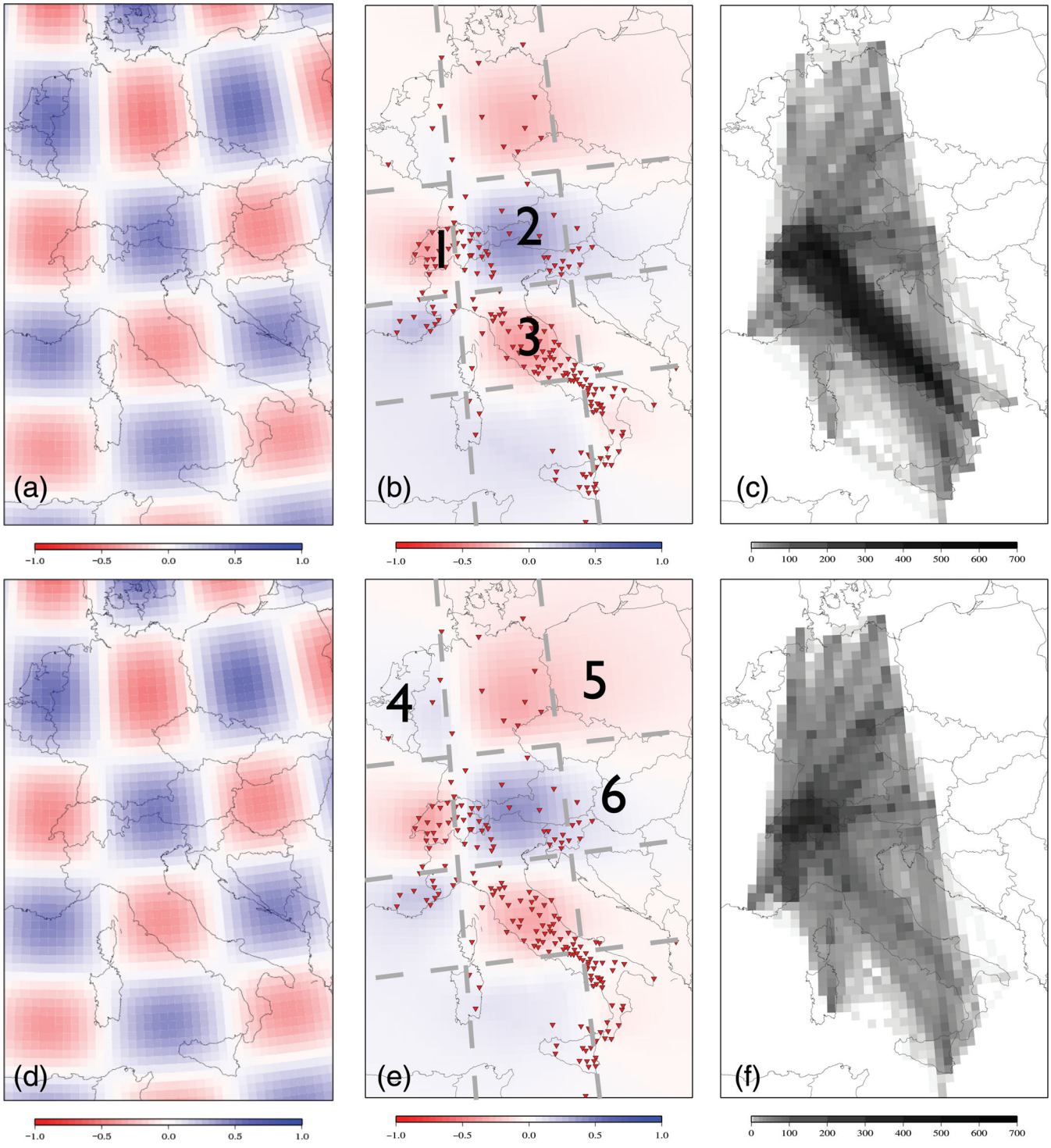

Figure 5. 'Checkerboard' test (a) and (d) Input model coinciding with the spherical harmonic function of degree 60 and order 30 and 1 per cent velocity anomalies (b) and (e) Output model obtained inverting a synthetic database associated with our 8 and 35 s Rayleigh-wave group velocity data set, and the input model at (a), (c) and (f) Density of ray paths associated with our measurements at 8 and 35 s Rayleigh-wave group velocity.

minimal length and up to 600 km length. We compute synthetic data and invert them as described earlier. The resulting models associated with 8, 16 and 35 s Rayleigh-wave group velocity data are shown in Fig. 6(b). Four images per period are show, one with the input model, one with the raw results, one with the results annotated for specific anomalies that are of interest and finally the result and the outlines of the well-resolved area as derived from this test. Fig. 6 shows that velocity heterogeneities of relative short length (100 km) can be resolved by our data coverage in those areas densely covered by stations namely Switzerland and northern Italy. In Germany, most longer-wavelength heterogeneities of 200 km or more are reproduced well, but most of the smaller scale features are lost. High-amplitude features of 150 km length are fairly well-resolved in southeastern France, Austria and southern Italy. The

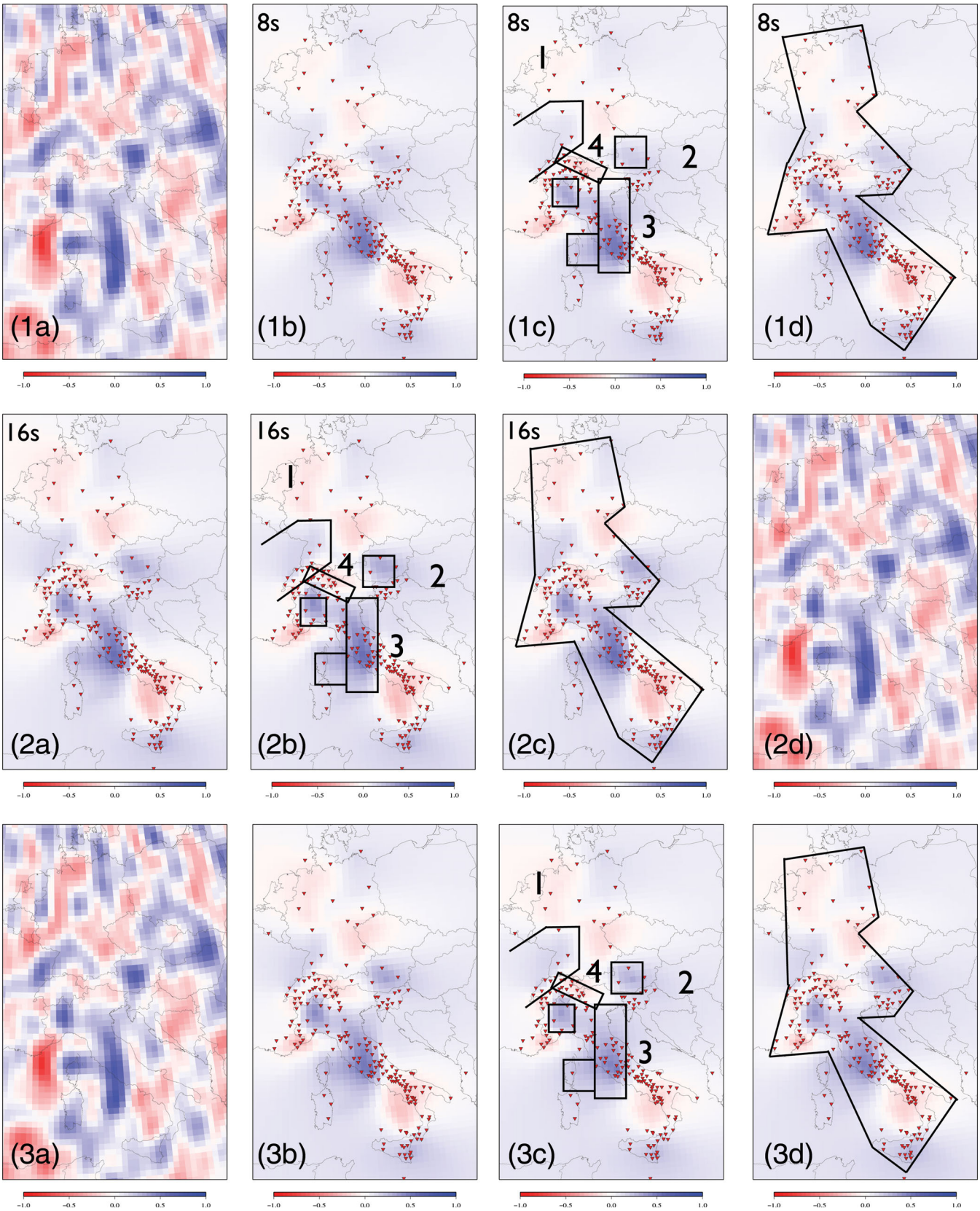

Figure 6. Synthetic test with randomly distributed velocity anomalies of various size as input: Panels 1(a), 2(d), 3(a) associated with our 8, 16 and 35 s Rayleigh-wave group velocity data set. Panels 1(b), 2(a) and 3(b): Raw output model associated with 8, 16 and 35 s, respectively. Panels 1(c), 2(b) and 3(c) Output models with outline of specific anomalies located inside the correct resolved part of the model. Panels 1(d), 2(c) and 3(d): Output model with the boundaries of the well-resolved area.

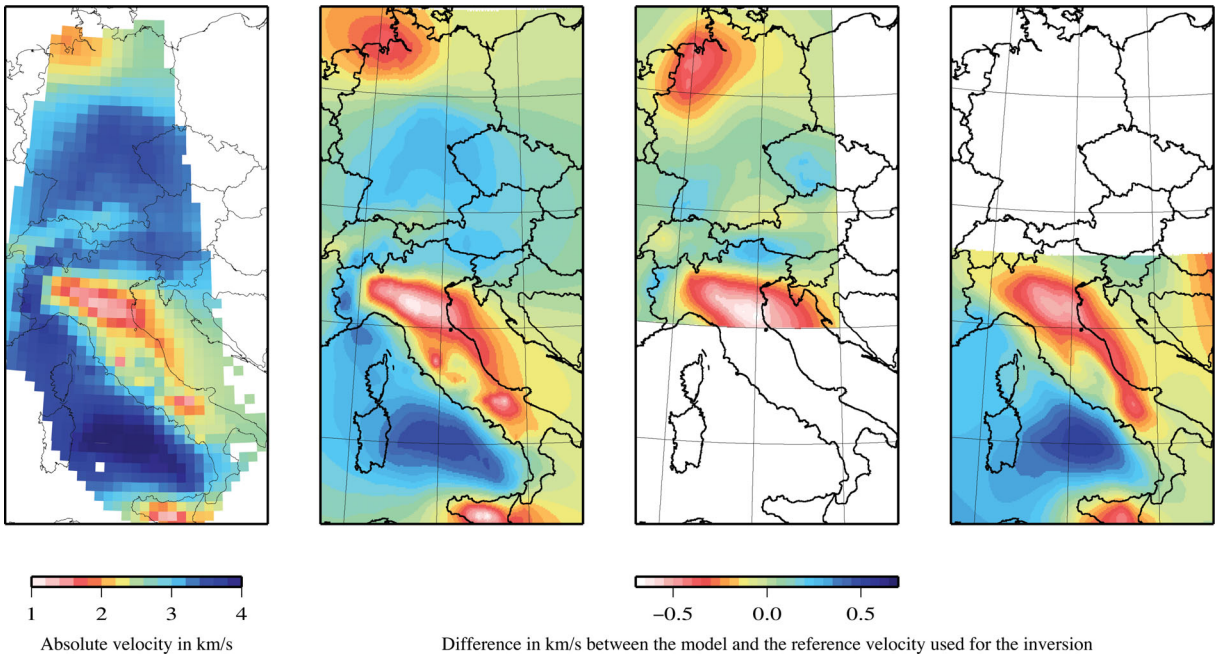

Figure 7. Rayleigh wave group-velocity map at 16 s period derived from our data set in km s^{-1}. (b) Same as (a) after removal of average velocity for better comparison it with other studies that used other reference velocities for the inversion. (c) and (d) Rayleigh-wave group-velocity maps derived from Stehly *et al.* (2009) and Li *et al.* (2010), respectively, after removal of average.

systematic underestimation of heterogeneity amplitude results from the damped least-square approach of inversion. More specifically, anomalies 1, 2 and 4 are fairly well resolved within the station array but the amplitudes are underestimated due to the lack of stations in that area. Anomaly marked 3 is an example of 100 km structure well-resolved with only limited reduction in amplitudes thanks to locally high-station density. The big square in Italy is well resolved, whereas in Corsica the shape of the anomaly is distorted and the amplitude is significantly reduced. Analysing the recovery of the velocity anomalies in all regions, one can draw the limitations of the well-resolved area and, for each period, we invert data from this information is incorporated in our interpretation. As an example the limits we draw for 8 s period and the one for 16 s period are globally similar in general but vary in the west of Germany, where at 8 s, the ray coverage is not sufficient.

To validate our results and our resolution estimates, we also compare them with those of previous studies from Stehly *et al.* (2009) and Li *et al.* (2010) as shown in Fig. 7. Fig. 7(a) shows the Rayleigh-group velocity map at 16 s derived from our data set in absolute velocity. The figure pixels coincide with pixels of our parametrization, so that the unsmoothed model is plotted. Fig. 7(b) shows the same result but after removing the mean and smoothing, as we smoothed the maps of Stehly *et al.* (2009) and Li *et al.* (2010) shown in Figs 7(c) and (d), respectively. The study by Stehly *et al.* (2009) includes data from 2004 to 2005 with station coverage limited to the northern portion of the region of interest. The study of Li *et al.* (2010) is based on the same data and station distribution as ours but limited to the Italian region. Even though the inversion process and data coverage differ, all studies show similar patterns of velocity anomalies. The Po Plain is visible and imaged at the same location by all studies. Our study and Li *et al.* (2010) show the same fast feature in the Tyrrhenian Sea caused by its thin crust resulting in surface wave energy propagating through the faster upper mantle. The results by Stehly *et al.* (2009) and ours show similar features in southern Germany, even though amplitudes are different. The Alpine region, from France to Slovenia also shows similar patterns in Figs 7(b) and (c), while the amplitudes differ. In general, the size of well-imaged features in all these studies is superior to 200 km, which is within the resolution limit of ray theory and that is about 100 km based on our synthetic tests.

3.2 Phase- and group-velocity tomography

We least-square invert our group- and phase-velocity data to derive the group- and phase-velocity maps shown in Figs 8 and 10, respectively. Data are selected before inversion, leaving out group- and phase anomalies associated with a SNR higher than 5 on cross-correlations. The inverse problem is non-unique and regularization must be applied to counter the effects of noise and of non-uniformities in data coverage. We select the weight of our regularization parameter (roughness damping only) small enough to provide a good recovery of the input model pattern (Section 3.1), but large enough to eliminate single-cell anomalies and sharp, small-scale heterogeneities that our data would not be able to resolve.

4 DISCUSSION

Rayleigh-wave group- or phase velocity can be thought of as the weighted average of heterogeneities in shear and compressional velocities and density, over a depth range that becomes wider with increasing surface wave period (e.g. Boschi & Ekstrom 2002). text removed as indicated by R2 The kernel functions that relate structure at depth with group- and phase velocity are dubbed ‘sensitivity functions’ and are discussed and illustrated. by Ritzwoller *et al.* (2001) and Fry *et al.* (2010). In the following, we interpret the maps of Figs 8 and 10 based on their sensitivity to structure at depth and expected geophysical features in different depth ranges.

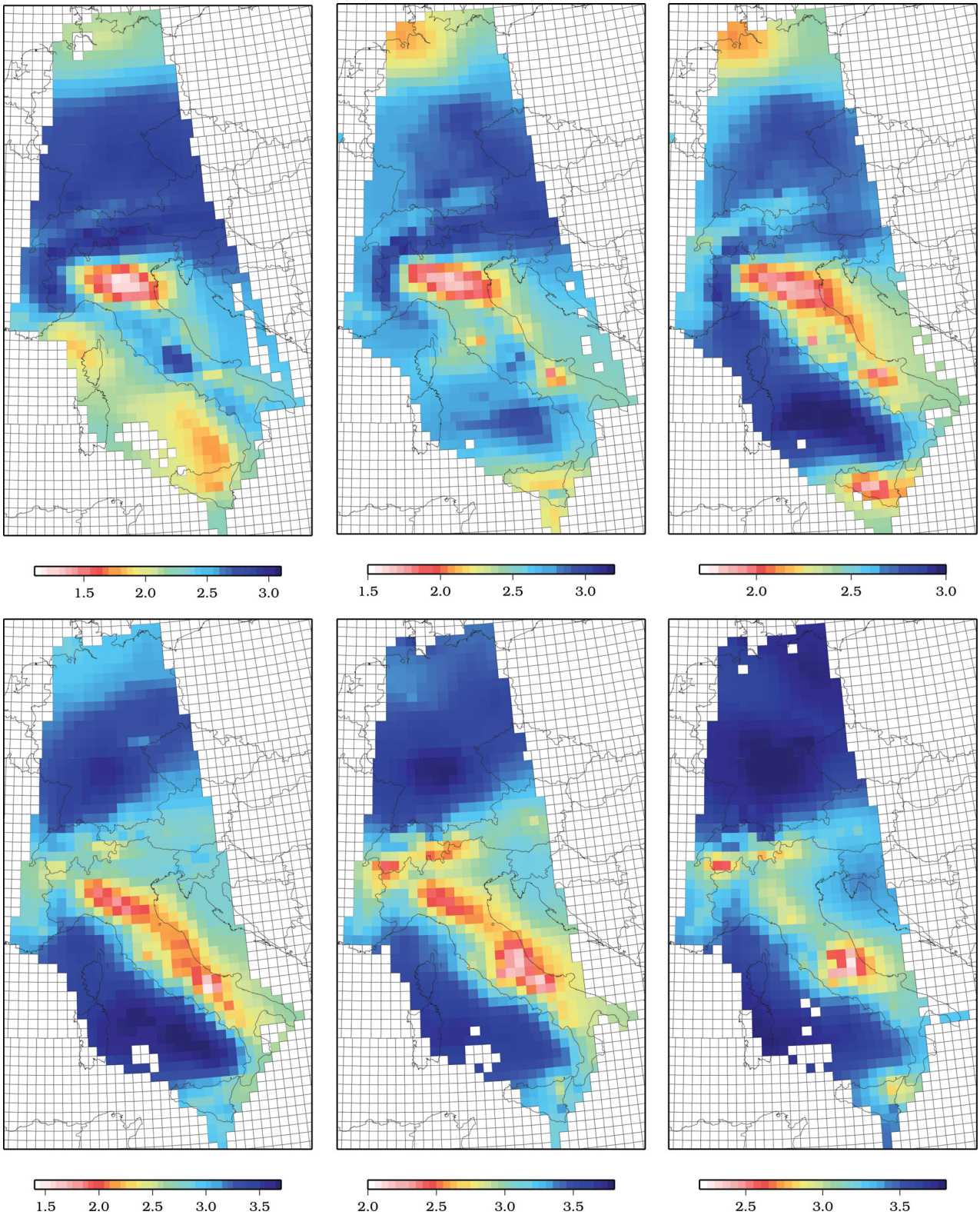

Figure 8. Group-velocity in km s^{-1} at (top, left- to right-hand panels) 8, 12, 16, (bottom, left- to right-hand panels) 24, 30 and 35 s periods, superimposed on our actual tomography parametrization grid. Velocity values are only plotted at pixels where there is at least one ray crossing the pixel.

4.1 Rayleigh-wave group velocity at 8 and 12 s periods

The propagation of 8 and 12 s surface waves is strongly affected by shallow crustal structure, with the maximum peak of sensitivity at 5 km depth and 8 km depth, respectively. One of the most prominent features of the 8 and 12 s group-velocity map of Fig. 8 is a low-velocity anomaly spanning the sedimentary basin associated with the Po plain, a WNW–ESE basin of sediments on average about 7 km thick. The Po Plain is filled by sediments originating mainly

from the Alps and to a lesser degree from the Apennines reaching a maximum thickness beneath the latter. Minimal group velocities here are as low as 1.4 km s^{-1}. Low velocities in sedimentary basins are expected based on the elastic properties of sediments. Another prominent feature are the Alps, which are imaged as a relative high-velocity anomaly in both the 8 and 12 s maps. This observation is consistent with the high shear velocities typically found at shallow depths in orogenic massifs. Lateral structure within Switzerland (the best covered area by our database) also confirms our resolution expectations: directly to the north of the Alps lies the Molasse sedimentary basin. Group velocities are quite high (up to 2.9 km s^{-1}) in Switzerland and over most of southern Germany with the exception of the Molasse basin running from Geneva to southern Bavaria (Munich). Compared to the Po Plain or other basin, sediments in the Molasse basin are more compacted, resulting in relatively fast wave propagation.

4.2 Rayleigh-wave group velocity at 16 s

Group-velocity maps at 16 s period are characterized by a number of different features with respect to shorter periods, which reflect the sensitivity of this surface wave mode to deeper structure whereas 8 and 12 s waves do not sample the mantle, 16 s ones do. Sensitivity of 16 s Rayleigh-wave group velocity is highest around 20 km depth, that is, in the mid/lower crust and, in some areas, the Moho. The main feature of the 16 s map is the high velocity mapped throughout the Tyrrhenian Sea, clearly associated with the thin oceanic crust of the area (e.g. Marone & Romanowicz 2007; Tesauro *et al.* 2008; Grad & Tiira 2009): in areas of thin crust, most surface wave energy is focused in the mantle rather than in the crust, and the higher shear velocity in the mantle defines the speed of surface wave propagation. In Germany and Switzerland, the geology around 20 km depth is analogous to that at shallow depths, and the 16 s map accordingly shows a similar pattern to the maps of 8 and 12 s. The Molasse basin in Germany is still visible which indicate that the upper crust is deep enough to affect 16 s waves. Further south, the Po plain is still prominent, consistent with the low shallow crust velocities observed in that area by Di Stefano *et al.* (2009). Other slow features, associated with the Apennines, are comparably important; low group velocities along the Apennines mountain range suggests that the underlying crust might be, at least locally, deeper than previously suggested. As a general rule, we find that features observed at 16 s are globally a mixture between upper crust and upper-mantle influence, whereas at shorter periods only the crust is relevant.

4.3 Rayleigh-wave group velocity at 24, 30 and 35 s

Longer-period group-velocity maps are overall characterized, as is to be expected, by higher velocities than their shorter period counterparts: with growing surface wave period, sensitivity is highest at larger depths where velocity beneath Moho exhibits a significant increase. Hence, maps in this period range are largely correlated to Moho topography depth, with anomalously high group velocity in areas of thin crust (particularly the Tyrrhenian Sea), and anomalously low velocities in areas of thick crust (the Alps and the Apennines). The Apennines show lower velocity and present a more prominent signature than the Alps. The Alps are narrower and run mostly E–W than the wider Apennines that run NW–SE. With sources mostly to the north, the waves are more affected by lower velocity structure while they travel through the Apennines than through the Alps. We also compare our group velocity maps with the Moho map of the Alpine region by Wagner *et al.* (2011) combining LET and CSS migrated information (Waldhauser *et al.* 1998, 2002) displayed in Fig. 9. We plot only the area in common to the two studies and we adapt our colourscale with low velocity in purple and fast velocity in yellow to allow better comparison. On the Moho map, the purple colour indicate deep Moho and yellow colour indicate shallow Moho. We clearly see that the two maps are in good general agreement. First, in the Alps where the Moho is deep, we observe very slow velocity with two peaks where the Moho is the deepest. Further south in Italy, beneath Emilia-Romagna and Marche, the same conclusion can be drawn though the positions of the slow velocity anomalies in our map are a bit shifted compared

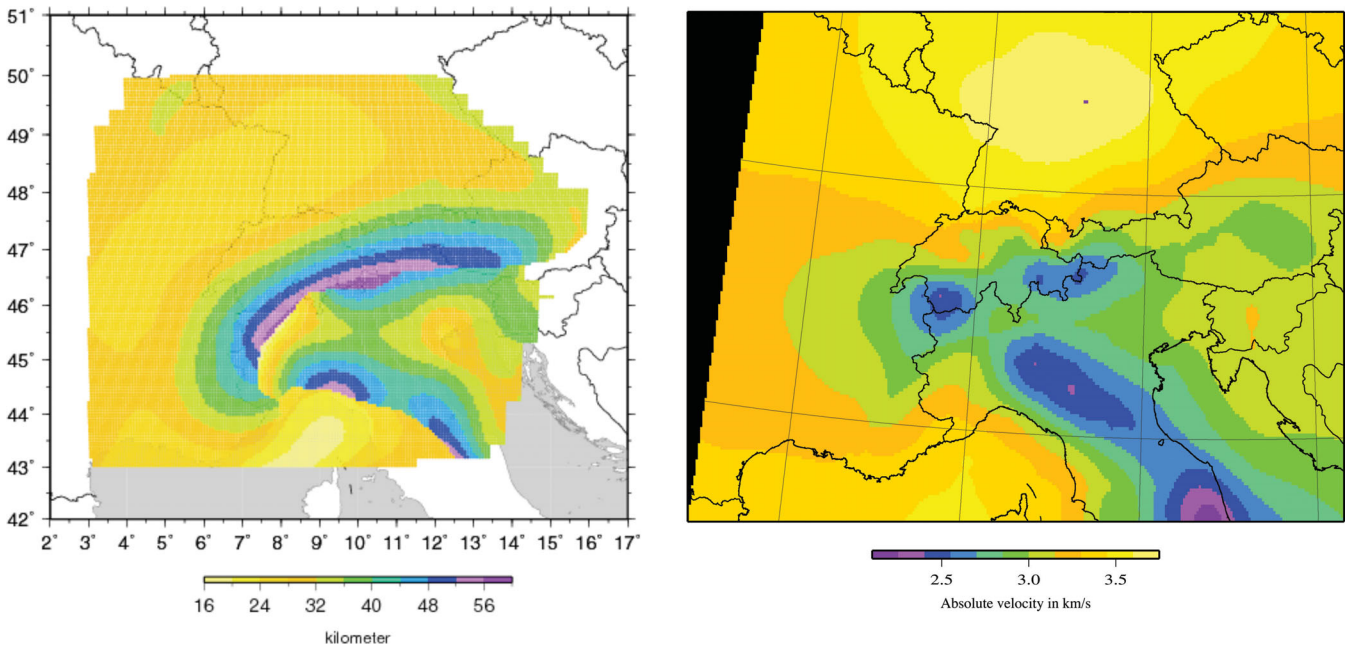

Figure 9. Left-hand panel: map of the Alpine Moho from Wagner *et al.* (2011). Right-hand panel: our Rayleigh-wave velocity map at 30 s with linear interpolation between the parametrization.

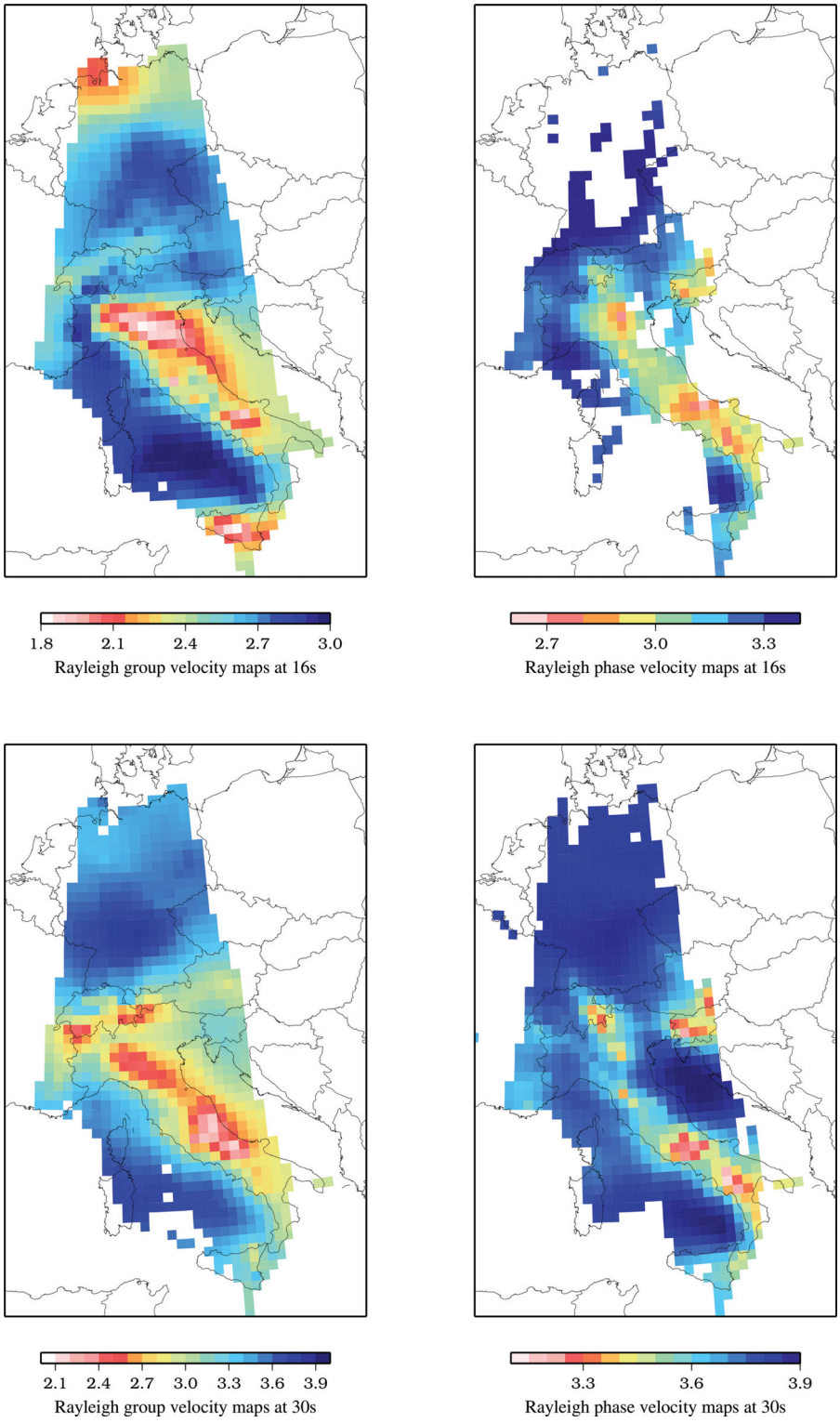

Figure 10. Group- (left-hand panel) and phase- (right-hand panel) velocity maps at 16 s (top panel) and 30 s (bottom panel) in km s^{-1}.

to the locations of deepest Moho in the Apennines according to Wagner *et al.* (2011). The Adriatic Moho topography, very steep towards the west of the Apennines, is hard to image by surface waves and could create this offset. Overall the two studies obtained by two different methods and approaches are in very good agreement, which confirms the reliability of our data set and results. The better performance of this study with respect to Stehly *et al.* (2009) in resolving Alpine structure at 30 s period is expected because our better station coverage south of the Alps and more in general, the wider aperture of our array: Pairs of relatively far-away stations contain the most long-period signal and will be particulary effective at providing observations of 30 s waves.

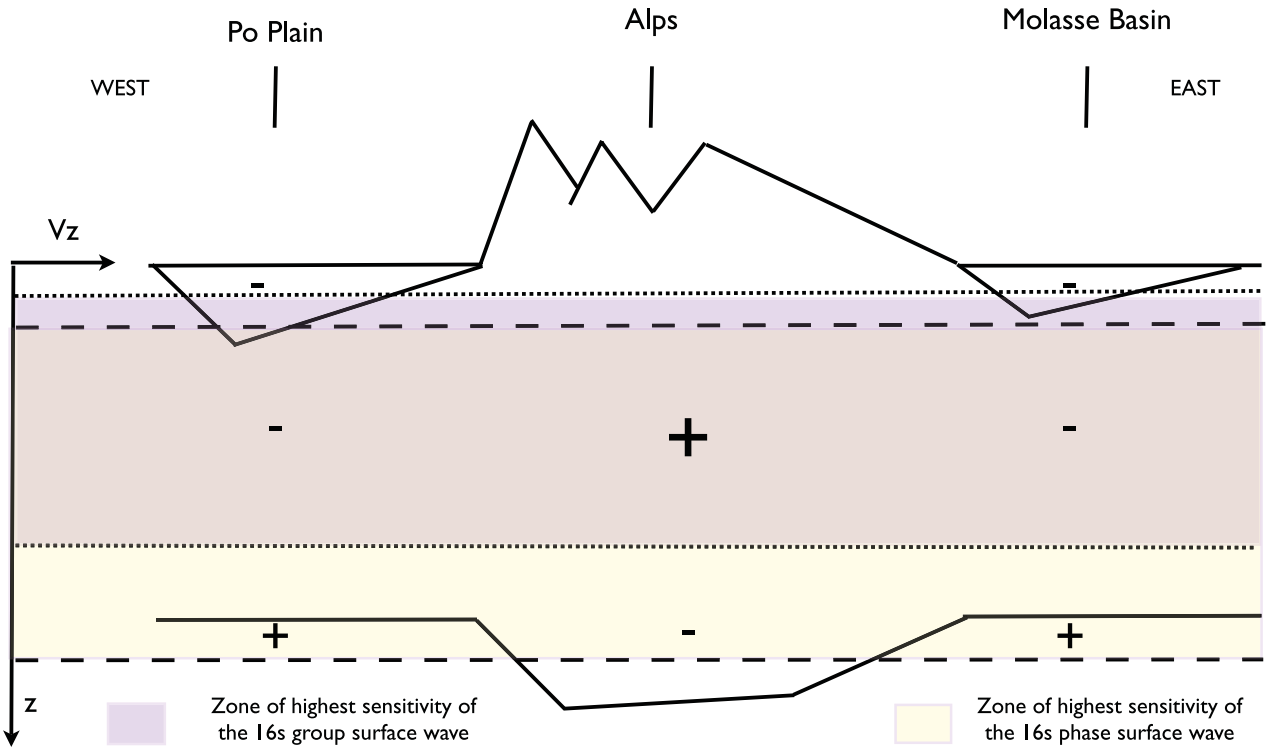

Figure 11. Schematic interpretation of the sensitivity area of both group and phase surface wave at 16 s beneath the Po Plain, the Alps and the south of Germany.

4.4 Rayleigh-wave phase-velocity maps

Our phase-velocity maps at 16 and 30 s are compared with the group-velocity map at the same period (Fig. 10). Based on Fig. 4 of Ritzwoller *et al.* (2001), group and phase velocities have different sensitivity to structure at depth. At any given period, group velocity samples a thinner and shallower layer than phase velocity and has an overall higher sensitivity to heterogeneities. This explains the difference in both amplitude and pattern between the left and right panels of Fig. 10. At 16 s, the Alps are characterized by higher group velocity than the Apennines whereas phase velocity is approximately the same. To explain this difference, we show in Fig. 11 a synthetic cross-section along the European GeoTraverse (EGT) from southern Germany to northern Italy. In the Molasse and Po basin, group velocity is low because its sensitivity is significant within the sediment layer. On the other hand, phase velocity only 'sees' the deepest part of the thicker Po Plain. Our 30 s phase-velocity map, also shown in Fig. 10, is clearly affected by Moho topography and by the seismic structure of mantle lithosphere (Lucente & Speranza 2001; Lippitsch *et al.* 2003; Panza & Raykova 2008), as is to be expected given the larger depth-range of sensitivity.

5 CONCLUSIONS

We assembled a high-quality database of group- and phase measurements in central Europe derived from ambient-noise cross-correlation and investigated the resolution power by synthetic tests using a characteristic model. In the region of dense station coverage (<40 km station spacing), the data set allows to resolve features as small as 100 or 200 km in areas of relatively poor station coverage (>100 km station spacing). We inverted our database to obtain maps of lateral variations in group- and phase-velocity heterogeneity throughout the region covered by the data. Comparing our results with those of earlier studies, we find, in general, very good correlation in region of higher station density, but our data set is able to resolve some structures in more detail. Based on sensitivity testing, we define the boundaries of regions with high sensitivity by our data set. Within this region, we identify in our maps a number of robust features that can be interpreted geophysically: namely, the Po-plain sedimentary basin, the thin crust of the Tyrrhenian Sea, the roots of the Alps and of the Apennines and the Molasse basin. Similar features were found, with somewhat lower resolution, in the earlier ambient-noise studies of Li *et al.* (2010) and Stehly *et al.* (2009). We also compare our 30 s Rayleigh-wave group velocity map with the new Moho map from Wagner *et al.* (2011) based on CSS and LET and find excellent correlation between the results obtained by the two different methods. Our results at longer periods document strong sensitivity to Moho topography, with low velocity in our map corresponding to thicker than average crust. In the near future, we will be able to infer from these data the 3-D shear-velocity structure of the region of interest and its pattern of azimuthal anisotropy as a function of depth, expanding the models of Stehly *et al.* (2009) and Fry *et al.* (2010). Surface wave ambient noise is the only seismically recorded signal to sample uniformly the crust–lithosphere depth range: collecting and interpreting these observations in terms of shear velocity structure is an important step towards the identification of a consensus tomographic model of the European crust and upper mantle.

ACKNOWLEDGMENTS

We are thankful to Jun Korenaga, Paul Cupillard and one anonymous reviewer for their useful comments and to Bill Fry for providing his

software as well as many helpful suggestions. This work would not have been possible without data provided by the Swiss Seismological Service, the INGV (in particular Fabrizio Bernardi) and the GRSN network.

REFERENCES

Basini, P., Nissen-Meyer, T., Boschi, L., Verbeke, J., Schenk, O. & Giardini, D., 2011. Ambient-noise tomography of the European lithosphere: numerical calculation of sensitivity kernels for non-uniform noise-source distributions, *Geophys. Res. Abstr.,* **13,** EGU2011-11554.

Bensen, G.D., Ritzwoller, M.H., Barmin, M.P., Levshin, A.L., Lin, F., Moschetti, M.P., Shapiro, N.M. & Yang, Y., 2007. Processing seismic ambient noise data to obtain reliable broad-band surface wave dispersion measurements, *Geophys. J. Int.,* **169**(3), 1239–1260.

Bijwaard, H. & Spakman, W., 2000. Non-linear global P-wave tomography by iterated linearized inversion, *Geophys. J. Int.,* **141**(1), 71–82.

Boschi, L., 2006. Global multiresolution models of surface wave propagation: comparing equivalently regularized Born and ray theoretical solutions, *Geophys. J. Int.,* **167**(1), 238–252.

Boschi, L. & Dziewonski, A.M., 1999. High- and low-resolution images of the Earth's mantle: implications of different approaches to tomographic modeling, *J. geophys. Res.,* **104**(B11), 25 567–25 594.

Boschi, L. & Ekstrom, R., 2002. New images of the Earth's upper mantle from measurements of surface wave phase velocity anomalies, *J. geophys. Res.,* **107**(B4), 2059, doi:10.1029/2000JB000059.

Boschi, L., Fry, B., Ekstrom, G. & Giardini, D., 2009. The European upper mantle as seen by surface waves, *Surv. Geophys.,* **30**(4-5), 463–501.

Boschi, L., Faccenna, C. & Becker, T.W., 2010. Mantle structure and dynamic topography in the Mediterranean basin, *Geophys. Res. Lett.,* **37**(20), L20303, doi:10.1029/2010GL045001.

Chang, S.J. *et al.*, 2010. Joint inversion for three-dimensional S velocity mantle structure along the Tethyan margin, *J. geophys. Res.,* **115**(B8), B08309, doi:10.1029/2009JB007204.

Chevrot, S., Sylvander, M., Benhamed, S., Ponsolles, C., Lefèvre, J.M. & Paradis, D., 2007. Source locations of secondary microseisms in western Europe: evidence for both coastal and pelagic sources, *J. geophys. Res.,* **112**(B12), B11301, doi:10.1029/2007JB005059.

Cupillard, P. & Capdeville, Y., 2010. On the amplitude of surface waves obtained by noise correlation and the capability to recover the attenuation: a numerical approach, *Geophys. J. Int.,* **181**(3), 1687–1700, doi:10.1111/j.1365–246X.2010.04586.x.

Di Stefano, R., Kissling, E., Chiarabba, C., Amato, A. & Giardini, D., 2009. Shallow subduction beneath Italy: three-dimensional images of the Adriatic-European-Tyrrhenian lithosphere system based on high-quality P wave arrival times, *J. geophys. Res.,* **114**(B5), B05305, doi:10.1029/2008JB005641.

Diehl, T., Deichmann, N., Kissling, E. & Husen, S., 2009. Automatic S-wave picker for local earthquake tomography, *Bull. seism. Soc. Am.,* **99**(3), 1906–1920.

Duvall, T.L., Jefferies, S.M., Harvey, J.W. & Pomerantz, M.A., 1993. Time distance helioseismology, *Nature,* **362**(6419), 430–432.

Dziewonski, A.M. & Anderson, D.L., 1981. Preliminary reference earth model, *Phys. Earth planet. Inter.,* **25**(4), 297–356.

Froment, B., Campillo, M., Roux, P., Gouedard, P., Verdel, A. & Weaver, R.L., 2010. Estimation of the effect of nonisotropically distributed energy on the apparent arrival time in correlations, *Geophysics,* **75**(5), SA85–SA93, doi:10.1190/1.3483102.

Fry, B., Deschamps, F., Kissling, E., Stehly, L. & Giardini, D., 2010. Layered azimuthal anisotropy of Rayleigh wave phase velocities in the European Alpine lithosphere inferred from ambient noise, *Earth planet. Sci. Lett.,* **297**(1-2), 95–102.

Gouédard, P., Roux, P., Campillo, M. & Verdel, A., 2008. Vergence of the two-points co-relation function toward the Green's function in the context of a prospecting dataset, *Geophysics,* **73**(2), V47–V53, doi:10.1190/1.3535443.

Grad, M. & Tiira, T., 2009. The Moho depth map of the European plate, *Geophys. J. Int.,* **176**(1), 279–292.

Harmon, N., Gerstoft, P., Rychert, C.A., Abers, G.A., de la Cruz, M.S. & Fischer, K.M., 2008. Phase velocities from seismic noise using beamforming and cross-correlation in Costa Rica and Nicaragua, *Geophys. Res. Lett.,* **35**(19), L19303, doi:10.1029/2008GL035387.

Herrin, E. & Goforth, T., 1977. Phase-matched filters—application to study of rayleigh-waves, *Bull. seism. Soc. Am.,* **67**(5), 1259–1275.

Husen, S., Diehl, T. & Kissling, E., 2009. The effects of data quality in local earthquake tomography: application to the Alpine region, *Geophysics,* **74**(6), WCB71–WCB79, doi:10.1190/1.3237117.

Kedar, S., Longuet-Higgins, M., Webb, F., Graham, N., Clayton, R. & Jones, C., 2008. The origin of deep ocean microseisms in the north atlantic ocean, *Proc. R. Soc.,* **464**(2091), 777–793.

Kissling, E., 1988. Geotomography with local earthquake data, *Rev. Geophys.,* **26**(4), 659–698.

Levshin, A.L., Yanovskaya, T.B., Lander, A.V., Bukchin, B.G., Barmin, M.P., Ratnikova, L.I. & Its, E.N., 1989. *Seismic Surface Waves in a Laterally Inhomogeneous Earth,* Modern Approaches in Geophysics Vol. 9, chapter 5, ed. Keilis-Borok, V.I., Kluwer, Dordrecht.

Li, H.Y., Bernardi, F. & Michelini, A., 2010. Surface wave dispersion measurements from ambient seismic noise analysis in Italy, *Geophys. J. Int.,* **180**(3), 1242–1252.

Lippitsch, R., Kissling, E. & Ansorge, J., 2003. Upper mantle structure beneath the Alpine orogen from high-resolution teleseismic tomography, *J. geophys. Res.,* **108**(B8), 2376, doi:10.1029/2002JB002016.

Lucente, F.P. & Speranza, F., 2001. Belt bending driven by lateral bending of subducting lithospheric slab: geophysical evidences from the northern Apennines (Italy), *Tectonophysics,* **337**(1-2), 53–64.

Marone, F. & Romanowicz, B., 2007. Non-linear crustal corrections in high-resolution regional waveform seismic tomography, *Geophys. J. Int.,* **170**(1), 460–467.

Meier, T., Dietrich, K., Stockhert, B. & Harjes, H.P., 2004. One-dimensional models of shear wave velocity for the eastern Mediterranean obtained from the inversion of Rayleigh wave phase velocities and tectonic implications, *Geophys. J. Int.,* **156**(1), 45–58.

Paige, C.C. & Saunders, M.A., 1982. LSQR—an algorithm for sparse linear-equations and sparse least-squares, *ACM Trans. Math. Softw.,* **8**(1), 43–71.

Panza, G.F. & Raykova, R.B., 2008. Structure and rheology of lithosphere in Italy and surrounding, *TerraNova,* **20**(3), 194–199, doi:10.1111/j.1365–3121.2008.00805.x.

Peter, D., Boschi, L. & Woodhouse, J.H., 2009. Tomographic resolution of ray and finite-frequency methods: a membrane-wave investigation, *Geophys. J. Int.,* **177**(2), 624–638.

Ritzwoller, M.H. & Levshin, A.L., 1998. Eurasian surface wave tomography: group velocities, *J. geophys. Res.,* **103**(B3), 4839–4878.

Ritzwoller, M.H., Shapiro, N.M., Levshin, A.L. & Leahy, G.M., 2001. Crustal and upper mantle structure beneath Antarctica and surrounding oceans, *J. geophys. Res.,* **106**(B12), 30 645–30 670.

Sanchez-Sesma, F.J. & Campillo, M., 2006. Retrieval of the Green's function from cross correlation: the canonical elastic problem, *Bull. seism. Soc. Am.,* **96**(3), 1182–1191.

Schivardi, R. & Morelli, A., 2009. Surface wave tomography in the European and Mediterranean region, *Geophys. J. Int.,* **177**(3), 1050–1066.

Schmid, S.M., Fugenschuh, B., Kissling, E. & Schuster, R., 2004. Tectonic map and overall architecture of the Alpine orogen, *Eclogae Geol. Helv.,* **97**(1), 93–117.

Shapiro, N.M., Campillo, M., Stehly, L. & Ritzwoller, M.H., 2005. High-resolution surface-wave tomography from ambient seismic noise, *Science,* **307**(5715), 1615–1618.

Snieder, R., 2004. Extracting the Green's function from the correlation of coda waves: a derivation based on stationary phase, *Phys. Rev. E, Stat. Nonlin. Soft Matter Phys.,* **69**(4), 46 610–46 618.

Stehly, L., Campillo, M. & Shapiro, N.M., 2006. A study of the seismic noise from its long-range correlation properties, *J. geophys. Res.,* **111**(B10), B10306, doi:10.1029/2005JB004237.

Stehly, L., Fry, B., Campillo, M., Shapiro, N.M., Guilbert, J., Boschi, L. & Giardini, D., 2009. Tomography of the Alpine region from observations of seismic ambient noise, *Geophys. J. Int.,* **178**(1), 338–350.

Tesauro, M., Kaban, M.K. & Cloetingh, S.A.P.L., 2008. EuCRUST-07: a new reference model for the European crust, *Geophys. Res. Lett.,* **35**(5), L05313, doi:10.1029/2007GL032244.

Tromp, J., Luo, Y., Hanasoge, S. & Peter, D., 2010. Noise cross-correlation sensitivity kernels, *Geophys. J. Int.,* **183**(2), 791–819.

Tsai, V.C., 2010. The relationship between noise correlation and the Green's function in the presence of degeneracy and the absence of equipartition, *Geophys. J. Int.,* **182**(3), 1509–1514.

Wagner, M., Kissling, E., Husen, S. & Giardini, D., 2011. Combining controlled-source seismology and local earthquake data to derive a consistent three-dimensional model of the crust: Application to the alpine region, *Geophys. Res. Abstr.,* **13,** EGU2011-8642.

Waldhauser, F., Kissling, E., Ansorge, J. & Mueller, S., 1998. Three-dimensional interface modelling with two-dimensional seismic data: the Alpine crust-mantle boundary, *Geophys. J. Int.,* **135**(1), 264–278.

Waldhauser, F., Lippitsch, R., Kissling, E. & Ansorge, J., 2002. High-resolution teleseismic tomography of upper-mantle structure using an a priori three-dimensional crustal model, *Geophys. J. Int.,* **150**(2), 403–414.

Wapenaar, K., 2004. Retrieving the elastodynamic Green's function of an arbitrary inhomogeneous medium by cross correlation, *Phys. Rev. Lett.,* **93**(25), 254 301/1–254 301/4.

Weaver, R., Froment, B. & Campillo, M., 2009. On the correlation of non-isotropically distributed ballistic scalar diffuse waves, *J. acoust. Soc. Am.,* **126,** 1817–1826, doi:10.1121/1.3203359.

Weaver, R.L.. & Lobkis, O.I., 2001. Ultrasonics without a source: thermal fluctuation correlations at MHz frequencies, *Phys. Rev. Lett.,* **87**(13), 134 301/1–134 301/4.

Yang, Y. & Ritzwoller, M., 2008. The characteristics of ambient seismic noise as as source for surface wave tomography, *Geochem. Geophys. Geosyst.,* **9**(4), Q02008, doi:10.1029/2007GC001814.

Yang, Y., Ritzwoller, M.H., Levshin, A.L. & Shapiro, N.M., 2007. Ambient noise rayleigh wave tomography across Europe, *Geophys. J. Int.,* **168**(1), 259–274, doi:10.1111/j.1365–246X.2006.03203.x.

Yao, H.J., Beghein, C. & van der Hilst, R.D., 2008. Surface wave array tomography in SE Tibet from ambient seismic noise and two-station analysis—II. Crustal and upper-mantle structure, *Geophys. J. Int.,* **173**(1), 205–219.